NUREG/CR-1634
LA-8475-MS
Informal Report
R1

Film Entrainment and Drop Deposition for Two-Phase Flow

A. Koestel*
R. G. Gido
J. S. Gilbert

Manuscript submitted: July 1980
Date published: August 1980

Prepared for
Division of Systems Integration
Office of Nuclear Reactor Regulation
US Nuclear Regulatory Commission
Washington, DC 20555

NRC FIN No. A7112

*Consultant. Box 108, Patagonnia Star Route, Buena Vista Ranch, Nogales, AZ 85621.

NOMENCLATURE

A	area
B	wave amplitude
C	entrained liquid concentration mass per unit volume
c_i'	imaginary part of complex wave propagation velocity
c_i	c_i'/u_2
c_R'	real part of complex propagation velocity
c_R	c_R'/u_2
D	tube diameter
d	drop or particle diameter
E	entrained liquid mass fraction
f	friction factor
G	mass velocity = flow rate/area
L	length
M	mass
$\dot{M}$	mass flow rate in axial direction
$\dot{m}$	mass transfer rate per unit surface area
R	Reynolds number
r	radius
S	correlating parameter used in Fig. 8
St_m	momentum transfer Stanton number
t	time
u	velocity in direction of flow
V_+	dimensionless particle deposition velocity
V_*	friction velocity = $(\tau/\rho_g)^{1/2}$
W	Weber number
x	quality
α'	wave number
α	$2\pi\delta/\lambda$
β	mass transfer coefficient, dimensions of velocity
δ	mean film thickness
ε_d	drop eddy diffusivity
ε_m	momentum eddy diffusivity
λ	wavelength
ρ	density
σ	surface tension
τ	shear stress
τ_t	turbulent shear stress
τ_+	dimensionless particle (drop) relaxation time
μ	viscosity
ν	kinematic viscosity

Subscripts

a	acceleration caused by body force
B	Blasius
d	deposition, drop
e	entrainment, equilibrium
f	film
F	flow direction
fn	neutral film
g	gas
i	interface
ℓ	liquid
m	momentum
t	turbulent
T	total
w	wall
2	liquid film interface
+	dimensionless mass deposition correlation parameter
0	initial value

FILM ENTRAINMENT AND DROP DEPOSITION FOR TWO-PHASE FLOW

by

A. Koestel, R. G. Gido, and J. S. Gilbert

ABSTRACT

A model for estimating the rate of film mass entrainment for drop-annular flow, based on film disturbance wave stability, was developed. The model was verified by application to tests involving deposition and entrainment. To account for the deposition, a recent particle mass diffusion correlation was used. Application of the entrainment and deposition models confirmed that a flow passage length (L/D) of about 100 or more is required to achieve near equilibrium, for a zero initial entrainment flow. The assumption of an initially fully entrained flow remaining approximately so, as used in nuclear power plant subcompartment analysis, is shown to be appropriate.

---

1. INTRODUCTION

This report presents a new basic model for the accounting of liquid film entrainment in drop-annular flow. This model then is combined with a more conventional, but current, model to account for drop deposition because most applications involve deposition and entrainment.

An understanding of the mechanics of entrainment and deposition often is essential for analysis of two-phase thermal-hydraulic problems. Such an understanding could be used to predict the (a) location where transition between annular flow and drop-annular flow occurs, (b) amount of liquid entrained from a film as a function of length, (c) flow passage length (L/D) required to achieve an equilibrium flow condition wherein the rate of deposition is balanced by the rate of film entrainment, and (d) deposition and subsequent entrainment from the deposited liquid film

It is surprising that the most elementary two-phase flow regime, annular flow, has turned out to be the most intractable to analyze or describe because

of the complexity of the gas-liquid interactions that occur. In addition, the entrainment field from liquid films is still in an unsatisfactory state. Important geometric variables are only dimly understood and the problem of designing and interpreting experiments is not yet satisfactorily solved.[1,2]

Our primary motivation for the development of these models concerned the deposition and entrainment that might occur in nuclear power plant subcompartments following a postulated loss-of-coolant accident (LOCA). Such considerations may be important in containment safety analysis.[3] For example, Refs. 4 and 5 indicate that homogeneous flow models required the assumption of partial deposition to improve the comparison between computer-calculated and LOCA-simulated test results.

Our entrainment model evolved from the concept, originally presented in Refs. 6 and 7, that the entrained drops result from the interfacial disturbance waves. Quantification of the concept is provided, in this paper, by the incorporation of empirical values for the film disturbance growth rate. The deposition model used is based on a current empirical correlation for the mass diffusion of particles (drops).

2. THEORY

The physical processes of film entrainment and drop deposition that we will represent are depicted in Figs. 1 and 2. Figure 1 shows the interfacial wave growth, instability, breakup into drops, and drop entrainment. Figure 2 could represent an equilibrium condition where the rate of liquid deposition equals the rate of liquid entrainment. This figure could also represent the deposition-dominated condition corresponding to the introduction of a dispersed flow if the liquid film and entrainment from the film are insignificant. In addition, Fig. 2 shows a possible formulation for the entrained liquid mass concentration (C) change over an incremental length. In the development below we will predict deposition rates from a general correlation for the mass diffusion. Recognition is given to the classic, but simple, mass diffusion model

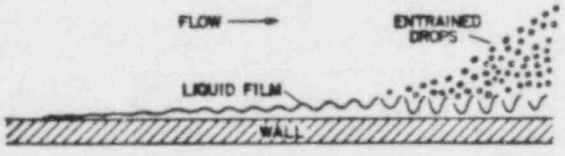

Fig. 1. The liquid film disturbance wave growth, instability, and breakup into drops schematic represents the gamut of wave types that might exist, such as waves with run under, beach-type waves, rib waves, and roll waves.

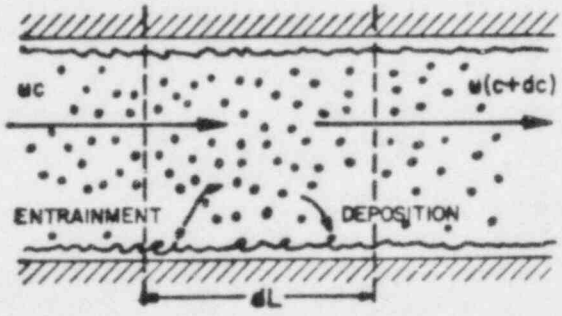

Fig. 2. Schematic representation of two-phase drop-annular flow with film entrainment and drop deposition.

based on the analogy between momentum and mass transfer. The entrainment phenomena analysis is based on the growth rate of the interfacial surface disturbance waves, whose crests atomize to form entrained drops. Gravity effects are assumed not to be of importance for the applications of interest.

2.1 Deposition

It is important to have a good basis for the extrapolation to large-scale applications of small-scale drop deposition correlations. A convenient starting point for computing drop deposition is to assume that the momentum analogy applies. It is known that the analogy has limitations for this application [8] but the analogy is useful as a basis for the explanation of deviations from the analogy.

For the analogy, the ratio of the drop or particle diffusivity (ε_d) is assumed to be equal to the fluid momentum diffusivity (ε_m). Particle deposition research has shown that the momentum analogy is a sound starting point for computing drop deposition with the understanding that there are many effects that cause deviations from the analogy. A prime factor involved in the deviations is the drop inertia.

Analysts have attempted to relate the ratio of the diffusivities ($\varepsilon_d/\varepsilon_m$) to the inertial behavior of the drops and the fluid turbulent eddies.[8-10] Some of these studies show that the turbulence imparted to the particles by the fluid is sometimes damped by the laminar sublayer as the particle approaches the wall.[8,11,12] The "Stokes Stopping Distance" and the "Saffman Lift Force" concepts explain the drop behavior in the laminar sublayer. Conversely, a sufficiently large drop inertia can almost completely negate the effect of the laminar sublayer.[13]

A measure of the inertia effect is the dimensionless particle relaxation time from Ref. 14,

$$\tau_+ = \frac{t_d V_*^2}{\nu_g} \quad , \qquad t_d = \frac{\rho_\ell d^2}{18\mu_g} \quad , \text{ and } \quad V_* = \sqrt{\frac{\tau}{\rho_g}} \quad , \tag{1}$$

where the drop diameter (d), drop density (ρ_ℓ), and transporting fluid viscosity (μ_g) define the particle relaxation time t_d and where the shear stress (τ) and density (ρ_g) define the friction velocity V_*. Figure 3, reproduced from Ref. 14, shows an experimental correlation of the dimensionless particle deposition velocity,

$$V_+ = \frac{\beta}{V_*} \quad , \tag{2}$$

vs the dimensionless particle relaxation time, where β is the mass transfer coefficient, which is also called the deposition velocity. The correlation of Fig. 3 is for a monodispersion of drop sizes and is supported by experimental data from several investigators. Note that V_+ represents the ratio of mass-to-momentum transfer as in the classical approach based on the analogy.

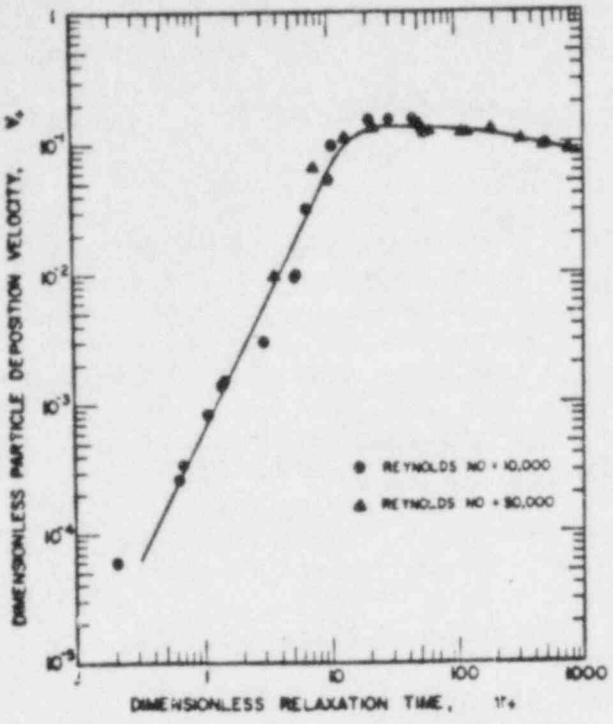

Fig. 3. Experimental relationship between the dimensionless particle deposition velocity and the dimensionless particle relaxation time (Ref. 14).

The advantages of a correlation such as that presented in Fig. 3 include the identification of the deposition regimes, the definition of the limitations of each regime, and the use of a correlating parameter involving the important inertia effect. The correlation shows that for $\tau_+ < 30$ a transition occurs in which the deposition rate decreases toward a regime controlled by Brownian diffusion.[15] At $\tau_+ = 30$, a maximum deposition rate corresponding to $V_+ = 0.15$ occurs, which agrees with the observations of Refs. 11 and 16. For values of $\tau_+ > 30$, the droplet inertia begins to reduce the ability of the drop to follow the fluid turbulence eddies and the drop deposition is reduced gradually.

Figure 3 shows that the deposition for a wide gamut of drop sizes can be represented by an approximately constant value of $V_+ = 0.15$. Two-phase flow experiments having a polydispersion of drop sizes confirm this assumption for engineering applications.[11,17] We will therefore assume that drop mass deposition can be represented by a constant value of $V_+ = 0.15$ with the qualification that the Brownian regime is not included, which is a good assumption for the applications of interest because the liquid-gas interface is probably turbulent.

The discussion above leads to the drop mass deposition rate per unit area ($\dot{m}_d$) given by

$$\dot{m}_d = \beta C = V_+ V_* C \quad , \tag{3}$$

where C is the bulk drop mass concentration per unit volume. A concentration of zero at the liquid interface is assumed.

The effect of a body force, such as that caused by gravity or acceleration, on drop deposition could be accounted for by using

$$\dot{m}_d = (\beta \pm \beta_a) C \quad ,$$

where β_a is the settling velocity due to the body force.

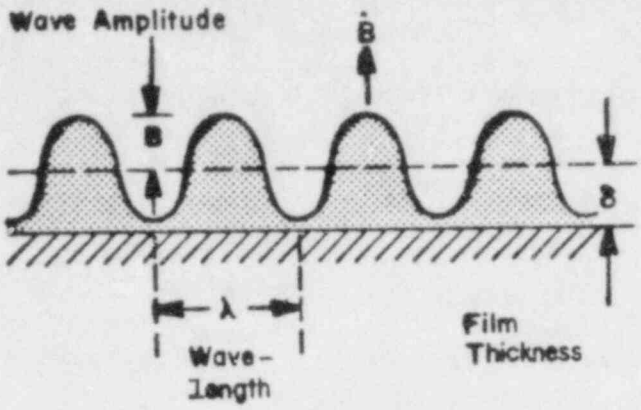

Fig. 4. Schematic of simplified wave characteristics showing wave growth with length.

2.2 Entrainment

Entrainment results from the continuous pumping of liquid into the gas core by means of interfacial wave growth. The wave crests generated are atomized by the flowing gas and the drops are entrained. This is consistent with experimental observation [18,19] and forms the basis of this analysis. Reference 6 presents an early discussion of this approach to the determination of film entrainment.

Figure 4 depicts the liquid film wave model used for our analysis. Let us assume that the rate of "pumping" liquid to the wave crests for atomization by the flowing gas can be represented approximately by the rate of wave amplitude growth over 2. This gives the liquid mass entrainment rate per unit area as

$$\dot{m}_e = \frac{\dot{B}\rho_\ell}{2} \quad . \tag{4}$$

As a result, the entrainment rate is coupled to the hydrodynamic characteristics of the film waves. This rate provides a necessary but not sufficient condition for determining entrainment. In addition, sufficient gas velocity to disperse the "pumped" liquid must exist.

When applying hydrodynamic stability theory to the liquid-vapor interface, a basic quantity, called the disturbance growth rate (αc_i), results. In the expression for the growth rate, $\alpha = 2\pi\delta/\lambda$, and $c_i = c_i'/u_2$, where c_i' is the imaginary part of the complex wave propagation velocity. When, (a) $c_i > 0$, instabilities result; (b) $c_i = 0$, stability is neutral; and (c) $c_i < 0$, damping occurs. Reference 6 shows that $\alpha' c_i' B = \dot{B}$, where $\alpha' = 2\pi/\lambda$. Combining these relationships with Eq. (4) gives

$$\dot{m}_e = \frac{B}{\delta}\,\alpha c_i u_2\,\frac{\rho_\ell}{2} \quad . \tag{5}$$

To apply Eq. (5), experimental values for (αc_i) must be used because theory based on the amplification of infinitesimal disturbances can give values for (αc_i) several magnitudes larger than experimentally observed. According to Ref. 6, the type of disturbance must be identified, i.e., Tollmien-Schlichting or Kelvin-Helmholtz, as well as the maximum growth rate. It usually is assumed that disturbances of all wavelengths are present and that the

wavelength giving the maximum growth rate dominates the interface. We have found that the Tollmien-Schlichting instability, which is characterized by the film Reynolds number, gives the maximum growth rate for liquid films flowing on walls for the air-liquid water system of interest to us. However, at low film Reynolds numbers and high gas velocities, atomization caused by the Kelvin-Helmholtz instability may become important and therefore the film Weber number would be an important parameter. For example, high-speed free liquid jets in the form of sheets or cylinders may be broken up by the Kelvin-Helmholtz instability. Note that the density and viscosity ratios of the two phases and the surface tension are inherent variables for determining growth rate. [6,20] Therefore, the application of a correlation based on one gas-liquid system must be used with caution when applied to another system.

One method of characterizing the wave parameters in Eq. (5) is to measure the mean liquid film thickness and the wave crest gradient of the interface as shown in Fig. 5. Then, the following equation from Ref. 6 can be applied.

$$\frac{dB}{dL} = \frac{B}{\delta} \frac{\alpha c_i}{c_R + 1} \quad . \tag{6}$$

Equation (6) is from Eq. (13) in Ref. 6, which also selected values of $c_R = 0.1$ and $\alpha = 0.6$. By measuring the slope dB/dL, values of $(B/\delta)\, c_i$ can be estimated. Reference 6 presents two such sample calculations based on Ref. 21 measurements. The measurements were used to obtain wave growth rates from the wave amplitude and film thickness measurements. The gas velocities of these experiments were less than that needed to atomize and entrain the liquid to facilitate the wave geometry measurements. Note that this approach to the characterization of the film to define entrainment is very direct and results in an equation for entrainment that is independent of the gas velocity, shear stress, etc.

Figure 6 is a plot of the maximum growth rate parameter vs the

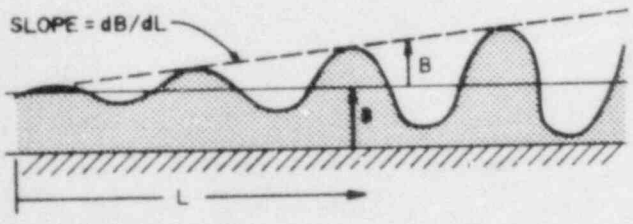

Fig. 5. Schematic of simplified wave characteristics showing wave growth with length.

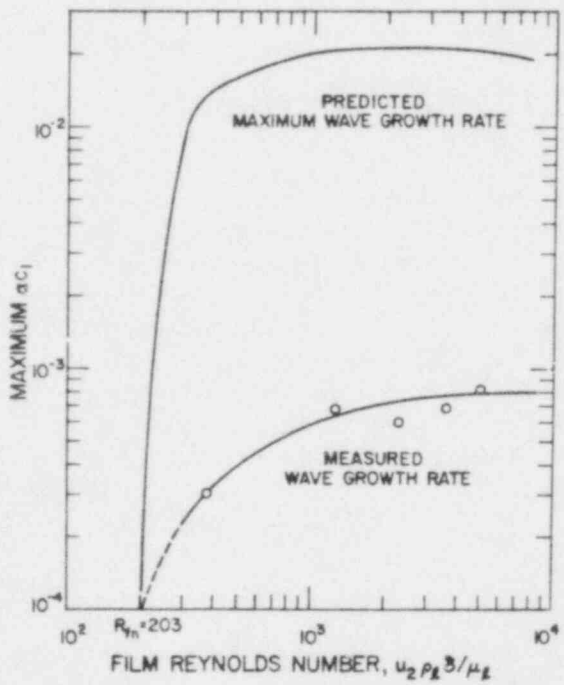

Fig. 6. Maximum wave growth parameter used in film entrainment model vs film Reynolds number, measured from Ref. 21, predicted from Ref. 20. Note, $R_{fn} = 203$ is the neutral stability film Reynolds number per Ref. 20.

film Reynolds number. The figure is based on the data of Ref. 21 and used to obtain the parameter as described above. The reference measurements also show that a suitable value for B/δ is 1, which was used in obtaining Fig. 6. However, values different from 1 also are possible according to Ref. 21. In Ref. 22, the maximum wave height and the mean film thickness were measured. These measurements show that for air-water flow the value of the ratio B/δ equals one for thin films and becomes greater than one as the film thickness increases. The experimentally indicated curve suggested by the measurements is compared with a predicted curve [6,2] that is based on small perturbation analysis. The order of magnitude difference between the theoretical and experimental results is not unusual. For example, the critical pipe Reynolds number based on the theory of disturbances of infinitesimal amplitude is 20 000 and the experimental value is 2 000. According to Miles,[20] the neutral stability film Reynolds number is 203, which is confirmed approximately by the data in Fig. 6.

Another method for the determination of the disturbance wave growth parameter (αc_i) is to use liquid entrainment measurements. However, this approach is indirect in that the combined effects of deposition and entrainment require accounting, which is compounded by the fact that most tests have not reached equilibrium where the rate of deposition and entrainment are equal. In addition, wave geometry, shear stress and gas velocity may be unknown. The comparison of the models and the experimental results (Sec. 3) uses entrainment measurements to confirm the disturbance wave growth correlation of Fig. 6.

2.3 Inception of Entrainment

For entrainment to occur, the liquid must be sufficiently unstable ($R_f > 203$) so as to pump liquid to the wave crests. In addition, the core gas velocity must reach a critical value large enough to atomize the liquid at the wave crests and to disperse it throughout the core. Based on measurements at the onset of entrainment for thin films, Ref. 23 gives the equation,

$$\frac{u_g \mu_g}{\sigma} \left(\frac{\rho_g}{\rho_\ell} \right)^{1/2} > 2.46 \times 10^{-4} ,$$

for the prediction of the critical velocity. This equation gives a value of 29 m/s for an air-water system at atmospheric pressure. Critical gas velocities near this value are indicated in Refs. 18 and 23.

3. COMPARISON OF MODELS WITH EXPERIMENTAL DATA

In this section, the models for entrainment and deposition developed previously and in Appendix A are used and evaluated by comparison with experimental results presented in Refs. 23 to 25. The results of Ref. 23 and 24 are used first to substantiate the entrainment parameter correlation of Fig. 6. Then, the models are applied to predict the results presented in Ref. 25.

3.1 Substantiation of Entrainment Model

The experimental results presented in Ref. 23 (p. 389) involve the downward flow of air and water in a 0.0222-m-diam tube. These results can be used

to verify the entrainment maximum wave growth rate parameter as postulated in Fig. 6. To do this, Eq. (A-6) for entrainment,

$$E = \frac{1}{2}\left[1 - \exp\left(-4V_+ \sqrt{St_m}\,\frac{L}{D}\right)\right]\frac{\beta}{\delta}\,\frac{\alpha c_i}{V_+\sqrt{St_m}}\left(\frac{\rho_\ell}{\rho_g}\right)^{1/2}\left(\frac{x}{1-x}\right), \qquad (7)$$

will be used. The parameter values to be used in this equation are discussed in the Appendices.

Another equation for entrainment (E) can be developed based on (1) the definition of E

$$E = \frac{\dot{M}_\ell - \dot{M}_{\ell f}}{\dot{M}_\ell},$$

(2) a liquid film mass flow rate ($M_{\ell f}$) for an average liquid flow velocity that is 7/8 of the liquid-gas interface velocity, and (3) a liquid film Reynolds number from

$$R_f = \frac{\rho_\ell u_2 \delta}{\mu_\ell}.$$

The resulting expression is

$$E = \left[1 - \frac{7}{2}\left(\frac{\mu_\ell}{\mu_g}\right)\frac{R_f}{R_T(1-x)}\right], \qquad (8)$$

where a total Reynolds number $R_T = G_T D/\mu_g$ is used. For known experimental flow, properties, and geometric conditions, Eqs. (7) and (8) become two equations involving E, R_f, and αc_i. The experimentally determined values of E result in the Ref. 23 data points plotted in Fig. 7.

The smooth-tube momentum transfer Stanton number,

$$St_m = \frac{0.023}{R_T^{0.2}},$$

with R_T based on total liquid and gas flows and gas viscosity, was used in the data reduction because measured flow resistance was not readily available. The Ref. 22 measurements of interfacial shear stress for air-water flow show that the ratio of u_g/V_* varies between 10 and 20, which corresponds to St_m values of 0.010 and 0.025, respectively. These values indicate that the liquid film-gas interface is rough.

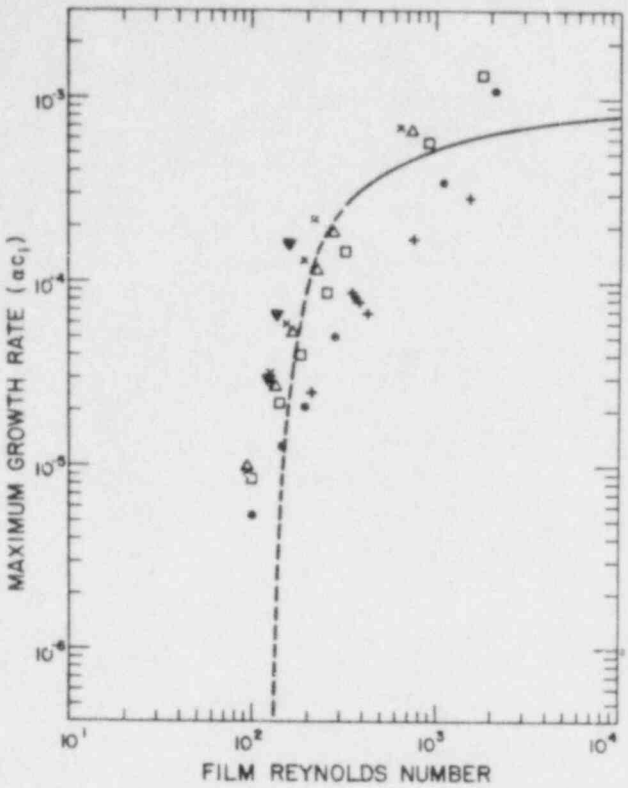

Fig. 7. Maximum wave growth rate parameter vs film Reynolds number for Ref. 23 (p. 389) data (• - 30, □ - 38, △ - 46, × - 53, ▼ - 61 m/s, superficial velocity) and for Ref. 24 data (+, 16-33 m/s superficial velocity). Curve is based on Ref. 21 film measurements, as shown in Fig. 6.

The presence of a wavy liquid film could have resulted in more flow resistance and a higher Stanton number. Higher values for αc_i would have resulted. However, it is possible that the film wave geometry also was different than assumed and lower values of αc_i would result if the wave amplitude to mean film thickness ratio (B/δ) was greater than the value of 1 used.

In general, the data of Ref. 23 confirm the proposed entrainment model as indicated by the clustering of the data points around the basic correlation from Fig. 6. The trend of the data also indicates an air velocity effect. This is speculated to be caused by the influence of velocity on the two-phase momentum Stanton number and not on the wave growth rate. The data deviations at a lower film Reynolds number could be caused by an increasing importance of the Kelvin-Helmholtz instability, as discussed in the entrainment section above. Note that the gas velocity is the superficial value, i.e., based on the total gas flow rate and the total tube area.

Recent measurements reported in Ref. 24 are included in Fig. 7. In this reference, the entrainment rate, $\dot{m}_e$, was determined from a mass balance involving the entrainment flow rate and drop deposition rate measurements. This unique approach allows the direct determination of the growth rate parameter, αc_i, from Eq. 5. The tests involved the upward flow of different liquids and air.

The data of Ref. 24 are for a superficial gas velocity 16 to 33 m/s. Since these gas velocities are near the critical values required for inception of entrainment (Sec. 2.3), it is not surprising that the data falls in the lower region of the correlation.

Reference 24 presents an empirical correlation in equation for for entrainment rate that includes the surface tension, interfacial shear and superficial film velocity. We have used this equation to show that the growth rate parameter αc_i, is a function of the liquid film Reynolds number and has a weak dependence on the gas velocity for a given liquid such as water. These characteristics of the data are implied in Fig. 7.

3.2 Application of Models to Data

In Ref. 25, approximate equilibrium measurements for annular flow of a liquid and a gas for large L/D experiments are described and correlated. Large L/D tests were selected so that near equilibrium conditions could be expected. In Appendix A, it is shown that this indeed was the case. Figure 8 shows the air-water data of this reference along with our predictions based on Eq. (A-2) of Appendix A. To make the comparison, the dimensionless group,

$$S = \frac{\tau_i \delta}{\sigma} ,$$

of the figure must be related to the Stanton number (St_m) of the equation to provide C_e as a function of S. This was accomplished in Appendix B by assuming that the interfacial shear stress (τ_i) is approximately equal to the wall shear stress (τ_w) for a thin turbulent liquid film and by assuming that the wavy liquid film can be represented as a film of uniform thickness. Appendix B gives the following relationship between St_m and S

$$\sqrt{St_m} = \left(\frac{\mu_\ell u_g}{\sigma}\right)^{1/6} \left(\frac{\rho_g}{\rho_\ell}\right)^{1/12} \frac{(0.0228)^{1/2}}{1.878} \frac{1}{S^{1/6}} \qquad (9)$$

Substituting this expression into Eq. (A-2) and letting the ratio $B/\delta = 1$ result in the C_e expression,

$$C_e = \frac{1.878}{(0.0228)^{1/2}} \frac{\rho_\ell}{2} \left(\frac{\rho_g}{\rho_\ell}\right)^{5/12} \frac{\alpha c_i}{V_+} \frac{S^{1/6}}{\left(\frac{\mu_\ell u_g}{\sigma}\right)^{1/6}} , \qquad (10)$$

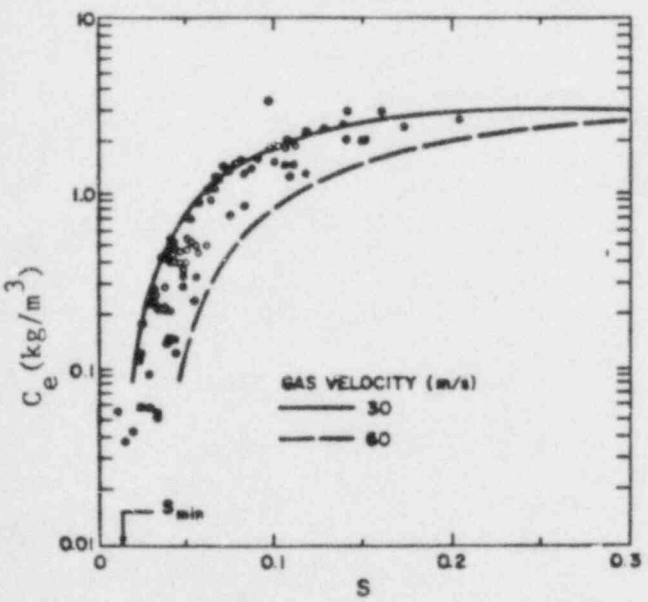

Fig. 8. Equilibrium air-water concentration correlation of Ref. 25, which is based on the dimensionless S parameter, compared with our predictions. S_{min} is for $W_{fn} = 2$ and $R_{fn} = 203$.

as plotted in Fig. 8. For comparisons with the air-water data of Ref. 25 this was readily accomplished because αc_i is a function of R_f as shown in Figs. 6 and 7 and S is also a function of R_f as given by Eq. (B-6) in Appendix B. Equation (10), as plotted in Fig. 8, provides a reasonable correlation of the air-water data for air velocities between 30 and 60 m/s, which are assumed to be representative of the experimental velocities. The agreement between the data and Eq. (10) indicates that the wave growth curves in Figs. 6 and 7 are supported by the experimental data of Fig. 8. Note that Eq. (10) shows a weak velocity effect as indicated by the data shown in Fig. 7.

The asymptotic value of the abscissa in Fig. 8 can be computed from the Blasius equation for shear stress in a turbulent liquid film [Appendix B, Eq. (B-4)].

Multiplying both sides of the Blasius equation by δ/σ produces the S parameter from Fig. 8 in the form

$$S = \frac{\tau\delta}{\sigma} = 0.0228\left(\frac{\delta\rho_\ell u_2^2}{\sigma}\right)\left(\frac{\nu}{u_2\delta}\right)^{1/4} = 0.0228\,\frac{W_{fn}}{R_{fn}^{1/4}} \quad .$$

Substitution of the neutral stability parameters for both the Kelvin-Helmholtz and Tollmien-Schlichting instabilities, i.e., $W_{fn} = 2$, $R_{fn} = 203$ (Ref. 6), results in $S = 0.012$. This value of S checks well with the data trend in Fig. 8. Values for the neutral stability film Weber and film Reynolds number (W_{fn} and R_{fn}) at the inception of entrainment, as tabulated in Ref. 6 from data obtained in Ref. 26, range from $R_{fn} = 113$ to 163 and $W_{fn} = 1.38$ to 2.05. These values approximately agree with the theory of Miles [20] and with the data trend in Fig. 8.

4. APPLICATIONS

Previous sections present models for the estimation of deposition and entrainment and verify the model predictability by comparison with experimental data. Application of the models is possible in several ways. For example, the entrainment model could be used for the case of all the liquid being on the wall with an exterior gas flow, from which the interfacial velocity would be determined for Eq. (5). Equation (3) for deposition would apply to flow where all of the liquid is entrained in the form of drops with no liquid on the wall. Combination of the entrainment and deposition models also could be done to analyze the situation where both phenomena exist. The latter approach could be done incrementally in a numerical analysis or on an integrated mean basis, as done in Appendix A.

An application of the models of particular interest is an evaluation of the 100% entrainment assumption conventionally made in nuclear power plant subcompartment pressure response analysis.[3-5] The assumption is based on the anticipation that the high-energy flows resulting from a LOCA produce a homogeneous two-phase mixture that will retain its homogeneity as the flow is distributed. Of course, there may be some slip flow caused by the pressure gradients at flow constrictions. The evaluation required consideration of the probable drop deposition and subsequent entrainment of the deposited liquid.

For the evaluation, deposition can be estimated by integrating Eq. (3) from an entrainment (E_0) of 1 to an entrainment of E for a corresponding L/D of 0 to L/D. This is done in a manner similar to the Appendix A integration for concentration. The change in entrainment resulting from the integration is

$$E = E_0 \exp\left(-4V_+ \sqrt{St_m}\,\frac{L}{D}\right) \qquad (11)$$

The effect on the entrained mass fraction of the entrainment of the deposited liquid with simultaneous continued deposition is given by Eq. (7), which combined with Eq. (11) results in

$$E = E_0 \exp\left(-4V_+ \sqrt{St_m}\,\frac{L}{D}\right) + \frac{1}{2}\left[1 - \exp\left(-4V_+ \sqrt{St_m}\,\frac{L}{D}\right)\right]\frac{B}{\delta}\,\frac{\alpha c_i}{V_+ \sqrt{St_m}}\left(\frac{\rho_\ell}{\rho_g}\right)^{1/2}\left(\frac{x}{1-x}\right) \quad . \qquad (12)$$

The use of Eq. (12) requires the growth rate parameter (αc_i), which is a function of the film Reynolds number, R_f, (Fig. 7). As for the small-scale experimental comparisons, we assume $\beta/\delta = 1$ and a smooth-tube Stanton number. The R_f is obtained from the mass balance represented by Eq. (8). A V_+ value of 0.15 per the deposition section is used.

For a given length (L/D) and flow conditions, the net entrainment (E) now can be determined. In particular, deposition is calculated first. Then the $\alpha c_i - R_f$ relationship of Fig. 7 is used with Eqs. (11) and (12) to calculate E.

Table 1 gives the geometry and flow conditions for representative subcompartment problems. In all cases, the flow lengths were too short for significant deposition to occur. It, therefore, followed that entrainment from the liquid film was correspondingly insignificant. As a result, the net fraction of liquid entrained in the main core was found to diminish little from the initial value E_0.

These analyses indicate the general validity of the conventional subcompartment analysis 100% entrainment assumption. This would be particularly true for flow regions near the break where the drops are thoroughly mixed and velocities are high. Other factors that may require consideration are the effects on deposition of obstacles, turning of flow, reduced velocity zones, and transient flow reversal.

5. SUMMARY

A new model for the estimation of the rate of film mass entrainment for drop-annular flow has been developed. The model is based on the stability of film disturbance waves. As a result of the model, key wave characterization parameters were identified and correlated on the basis of film wave measurements. Further resolution of the film wave characteristics based on detailed wave measurements is still required. The entrainment model has been verified by application to tests that involved deposition and entrainment.

The comparisons with tests involving deposition required an accounting for the mass deposition rate. To provide this, a current correlation for particle mass diffusion was used. The correlation is convenient because of its insensitivity to drop (particle) sizes over a wide range of sizes.

TABLE 1

REPRESENTATIVE SUBCOMPARTMENT PROBLEMS

	Problem				
	A	B	C	D	E
Geometry--					
Length (m)	5.3	11.3	24.	10.	10.
Hydraulic Diameter (m)	2.6	5.6	12.	1.8	1.1
Flow conditions--					
Quality,[a] x	0.43	0.43	0.43	0.38	0.47
Mass Velocity, $kg/s/m^2$	3.4×10^3	235	844	72	12×10^3
Source Ref. No.	----------27----------			28	29
Problem Description	--------Analytical-------- Std. Probs. 1 4 10			Test C-5	Typical Subcompartment Analysis

[a]Based on isenthalpic expansions of 1.28 to 1.51 MJ/kg saturated liquid to atmospheric pressure.

The combined entrainment and deposition models have been used in comparisons with test measurements. The comparisons are favorable and supportive of the models proposed. In addition, the combined accounting for entrainment and deposition allows the estimation of (1) the L/D required to achieve equilibrium of the two processes when the flow is initially at zero entrainment and (2) the extent of deviation from full entrainment of a flow whose liquid is initially fully entrained. The combined accounting reveals that (1) an L/D of about 100 or more is required to achieve near equilibrium and (2) the assumption of an initially fully entrained flow remaining approximately so, as used in nuclear power plant subcompartment analysis, is appropriate.

ACKNOWLEDGMENT

This work was supported by the U.S. Nuclear Regulatory Commission, Division of Systems Integration.

APPENDIX A

COMBINED DEPOSITION AND ENTRAINMENT

1. EQUILIBRIUM CONDITION

The section on entrainment gives Eq. (5)

$$\dot{m}_e = \frac{B}{\delta} \alpha c_i u_2 \frac{\rho_\ell}{2} \quad ,$$

and the section on deposition gives Eq. (3) for deposition

$$\dot{m}_d = \beta C = V_+ V_* C \quad .$$

The friction velocity (V_*) is expressed as

$$V_* = \sqrt{\frac{\tau}{\rho_g}} \quad .$$

Using the momentum Stanton number,

$$St_m = \frac{\tau}{\rho_g u_g^2} = \frac{f}{2} \quad ,$$

where u_g is the gas velocity, the mass deposition rate becomes

$$\dot{m}_d = V_+ u_g \sqrt{St_m}\, C \quad .$$

At equilibrium, the mass deposition rate equals the mass entrainment rate resulting in

$$C_e = \frac{B}{\delta} \frac{\alpha c_i}{V_+ \sqrt{St_m}} \left(\frac{u_2}{u_g}\right) \frac{\rho_\ell}{2} \quad . \qquad \text{(A-1)}$$

Using the conservation of momentum across the gas-liquid interface the equilibrium concentration becomes

$$C_e = \frac{B}{\delta} \frac{\alpha c_i}{V_+ \sqrt{St_m}} \left(\frac{\rho_g}{\rho_\ell}\right)^{1/2} \frac{\rho_\ell}{2} \quad . \tag{A-2}$$

An expression for the equilibrium liquid entrainment mass fraction also is useful. The entrainment, for a void fraction near 1, is

$$E = \frac{Cu_g A}{\dot{M}_\ell} = \frac{C\dot{M}_g}{\dot{M}_\ell \rho_g} \quad .$$

From Eq. (A-2), then,

$$E_e = \frac{1}{2} \frac{B}{\delta} \frac{\alpha c_i}{V_+ \sqrt{St_m}} \left(\frac{\rho_\ell}{\rho_g}\right)^{1/2} \frac{\dot{M}_g}{\dot{M}_\ell} \quad . \tag{A-3}$$

Using

$$\frac{\dot{M}_g}{\dot{M}_\ell} = \frac{x}{(1 - x)} \quad ,$$

results in

$$E_e = \frac{1}{2} \frac{B}{\delta} \frac{\alpha c_i}{V_+ \sqrt{St_m}} \left(\frac{\rho_\ell}{\rho_g}\right)^{1/2} \frac{x}{(1 - x)} \quad . \tag{A-4}$$

2. NONEQUILIBRIUM

The case in which entrainment and deposition rates are not equal is of practical interest. It has been observed experimentally that several hundred diameters in tube length are required to approach equilibrium. Consider a

liquid mass balance on the gas core, schematically shown in Fig. 2. The liquid mass entering the control volume is

$$u_g C \frac{\pi D^2}{4} + \dot{m}_e \pi D \, dL \quad ,$$

and that leaving is

$$u_g (C + dC) \frac{\pi D^2}{4} + \dot{m}_d \pi D \, dL \quad .$$

Using our deposition and entrainment equations gives

$$dC = \left(\frac{B}{\delta} \alpha c_i \frac{u_2}{u_g} \frac{\rho_\ell}{2} - V_+ \sqrt{St_m} \, C \right) \frac{4 \, dL}{D} \quad .$$

Integrating from L = 0 to L and from C = 0 to C with other parameters constant results in

$$\frac{C}{C_e} = 1 - \exp \left(-4 V_+ \sqrt{St_m} \frac{L}{D} \right) \quad . \qquad \text{(A-5)}$$

It can be shown that $C/C_e = E/E_e$.

As an example of the use of Eq. (A-5), consider the assumption of Ref. 25 that an L/D of 150 results in approximate equilibrium conditions. Using a smooth-tube gas-only Stanton number relation, along with a Reynolds number of 10^5 gives

$$St_m = \frac{0.023}{R_T^{0.2}} = 0.0023 \quad .$$

Then, using $V_+ = 0.15$ results in $C/C_e = 0.987$, which verifies the assumption.

A nonequilibrium expression for the fraction of total liquid mass entrained is also of interest. Following the development of Eq. (A-4) and using Eq. (A-5) produce

$$E = \frac{1}{2}\left[1 - \exp\left(-4V_+ \sqrt{St_m}\,\frac{L}{D}\right)\right]\frac{B}{\delta}\,\frac{\alpha c_i}{V_+\sqrt{St_m}}\left(\frac{\rho_\ell}{\rho_g}\right)^{1/2}\left(\frac{x}{1-x}\right) \quad . \tag{A-6}$$

Note that

$$E_e = \frac{B}{\delta}\,\frac{\alpha c_i}{V_+\sqrt{St_m}}\left(\frac{\rho_\ell}{\rho_g}\right)^{1/2}\left(\frac{x}{1-x}\right) \quad . \tag{A-7}$$

APPENDIX B

S PARAMETER ACCOMMODATION IN FIG. 8

A comparison of our proposed model and the experimental results of Ref. 25 is presented in Sec. 3. To do this, the reference S parameter,

$$S = \frac{\tau_i \delta}{\sigma} \quad ,$$

required manipulation into an expression that was consistent with our model parameters. This was accomplished by assuming that the interfacial liquid velocity of a thin turbulent liquid film corresponds to the velocity at the edge of a boundary layer, see Fig. B-1. As a result, the following equations (p. 146 of Ref. 30),

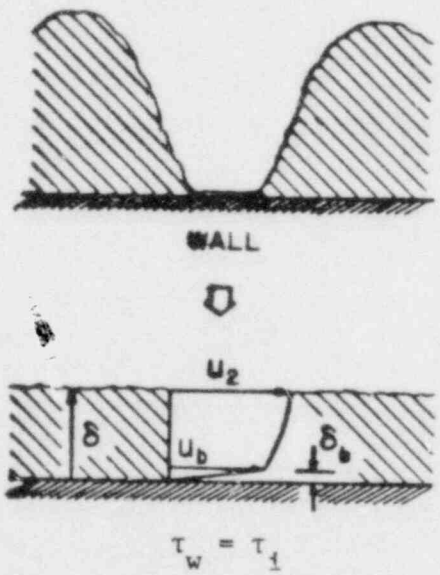

Fig. B-1. Approximate representation of a wavy liquid film by a constant thickness film on which a boundary layer relationship between velocity and film height is performed.

$$\tau = \mu_\ell \frac{u_b}{\delta_b} \quad , \tag{B-1}$$

$$\frac{\delta_b}{\delta} = \left(\frac{u_b}{u_2}\right)^7 \quad , \text{ and} \tag{B-2}$$

$$\frac{u_b}{u_2} = \frac{1.878}{R_f^{1/8}} \quad , \tag{B-3}$$

are applicable and can be used to develop relationships between S and R_f and between S and St_m. In addition, the Blasius equations (Eq. 143 of Ref. 30)

$$\tau = 0.0228\, \rho_\ell\, u_2^2 R_f^{-1/4} \quad , \tag{B-4}$$

and the slip ratio based on the conservation of momentum,

$$\frac{u_2}{u_g} = \left(\frac{\rho_g}{\rho_2}\right)^{1/2} \quad , \tag{B-5}$$

are used. A combination of Eq. (B-1) minus Eqs. (B-3) and (B-5) results in

$$S = \frac{R_f^{3/4}}{(1.876)^6}\left(\frac{\mu_\ell u_g}{\sigma}\right)\left(\frac{\rho_g}{\rho_\ell}\right)^{1/2} \quad . \tag{B-6}$$

To form the Stanton number for momentum ($St_m = \tau/\rho_g u_g^2$), Eqs. (B-4), (B-6), and (B-5) are combined to give

$$(St_m)^{1/2} = \frac{(0.0228)^{1/2}}{1.878}\left(\frac{\mu_\ell u_g}{\sigma}\right)^{1/6}\left(\frac{\rho_g}{\rho_\ell}\right)^{1/12} S^{-1/6} \quad . \tag{B-7}$$

Substituting Eq. (B-7) into Eq. (A-2) and letting $B/\delta = 1$, result in

$$C_e = \frac{1.878}{(0.0228)^{1/2}}\left(\frac{\sigma S}{\mu_\ell u_g}\right)^{1/6} \frac{\rho_\ell}{2}\left(\frac{\rho_g}{\rho_\ell}\right)^{5/12}\left(\frac{\alpha c_i}{V_+}\right) \quad . \tag{B-8}$$

Equation (B-8) is plotted in Fig. 8 for the comparison with the test data of Ref. 25.

To better understand the use of the relationships developed, a sample calculation for representative conditions of Ref. 25 is now presented. For

the flow of air and water, the properties are

$\rho_\ell = 1\ 000\ kg/m^3$, $\sigma = 0.073\ N/m$,

$\rho_g = 2.22\ kg/m^3$, and $\mu_\ell = 0.00114\ N \cdot s/m^2$.

Assume an air velocity (u_g) of 30 m/s and a deposition parameter V_+ of 0.15 (see Sec. 2.1). Selecting an $R_f = 2\ 000$ gives $\alpha c_i \cong 1 \times 10^{-3}$ from Fig. 7 and a value of $S = 0.15$ results from Eq. (B-6). A corresponding equilibrium concentration for comparison with the experimental data of $C_e = 2.68\ kg/m^3$ results from Eq. (B-8), see Fig. 8.

REFERENCES

1. Griffith, P., and Tong, L.S., "Two-Phase Flow Heat Transfer," American Institute of Chemical Engineers Today Series, 1973.
2. Ginoux, J. J., Ed., Two-Phase Flows and Heat Transfer with Applications to Nuclear Reactor Design Problems (Hemisphere Publishing Co., Washington, D.C., 1978).
3. "Standard Review Plan for the Review of Safety Analysis Reports for Nuclear Power Plants," Sec. 6.2.1.2, Office of Nuclear Reactor Regulation, U.S. Nuclear Regulatory Commission report NUREG-75/087, LWR Edition, September 1975.
4. Kanzleiter, T. F., "LOCA Experiments with a PWR-Multicompartment Model Containment," American Nuclear Society Thermal Reactor Safety Meeting, Sun Valley, ID, July 31-August 4, 1977.
5. Gido, R. G., Gilbert, J. S., and Jensen, W. L., "Containment Ice-Condenser Analysis using the COMPARE Code," American Nuclear Society Thermal Reactor Safety Meeting, Sun Valley, ID, July 31-August 4, 1977.
6. Koestel, A. and Smith, C. M., "Radiator Design Limitations for Dynamic Converters," Sixth AGARD Combustion and Propulsion Colloquium, Cannes, France, March 1964.
7. Ostrach, S. and Koestel, A., "Film Instabilities in Two-Phase Flows," American Institute of Chemical Engineers Journal, August 1963.
8. Hutchinson, P., Hewitt, G. F., and Dukler, A. E., "Deposition of Liquids or Solid Dispersions from Turbulent Gas Streams: A Stochastic Model," Chem. Eng. Sci. 26, 419-439 (1971).
9. "High-Speed Aerodynamics and Jet Propulsion," in Combustion Processes (Princeton University Press, 1956), Vol. II, Sec. J.
10. Rouhainen, P. O. and Stachiewicz, J. W., "On the Deposition of Small Particles from Turbulent Steams," Journal of Heat Transfer, February 1970.
11. Ganić, E. N. and Rosenhow, W. M., "On the Mechanism of Liquid Drop Deposition in Two-Phase Flow," American Society of Mechanical Engineers paper 76-WA/HT-18, December 1976.
12. Forney, L. J. and Spielman, L. A., "Deposition of Coarse Aerosals from Turbulent Flows," in Aerosol Science (Pergamon Press, Great Britain, 1974), Vol. 5.

13. Cousins, L. B. and Hewitt, G. F., "Liquid Phase Mass Transfer in Annular Two-Phase Flow: Droplet Deposition and Liquid Entrainment," Atomic Energy Research Establishment report R 5657, Harwell Berkshire, United Kingdom, 1968.
14. Liu, B. Y. H. and Agarwal, J. K., "Experimental Observations of Aerosal Deposition in Turbulent Flow," in Aerosol Science (Pergamon Press, Great Britain. 1974) Vol. 5.
15. Einstein, A., Vol. 17, Annals of Physics, pp. 549-560, 1905.
16. Gardiner, G. C., "Brief Communication--Deposition of Particles from a Gas Flowing Parallel to a Surface," International Journal of Multiphase Flow, Vol. 2, 1975.
17. Iloeje, O. C., Plummer, D. N., Rosenhow, W. M., and Griffith, P., "A Study of Wall Rewet and Heat Transfer in Dispersed Vertical Flow," Massachusetts Institute of Technology technical report 72718-92, September 1974.
18. "Water Entrainment in Nuclear Reactor Intercompartment Flow," Electric Power Research Institute report EPRI 275-1, October 1975.
19. Langner, H., "Studies of the Entrainment Behaviour in Steady and Transient Two-Phase Annular Flow," Doctor of Engineering Thesis, University of Hannover, West Germany, 1978, Los Alamos Scientific Laboratory translation LA-TR-78-43.
20. Miles, J. W., "The Hydrodynamic Stability of a Thin Film in Uniform Shearing Motion," Journal of Fluid Mechanics, Vol. 8, Part 4, pp. 593-611, 1960.
21. Chien, S. F., "An Experimental Investigation of the Liquid Film Structure and Pressure Drop of Vertical, Downward Annular Two-Phase Flow," University of Minnesota Ph.D. Thesis, April 1961.
22. Hori, K., Nakazatomi, M., Nishikawa, K., and Sekoguchi, K., "On Ripple of Annular Two-Phase Flow - 3. Effect of Liquid Viscosity on Characteristics of Wave and Interfacial Friction Factor," Bulletin of the Japanese Society of Mechanical Engineers, Vol. 22, No. 169, pp. 952-959 (July 1979).
23. Wallis, G. B., One-Dimensional Two-Phase Flow," (McGraw-Hill, NY, 1969) Sec. 12.
24. Ueda, T., "Entrainment Rate and Size of Entrained Droplets in Annular Two-Phase Flow," Bulletin of the Japanese Society of Mechanical Engineers, Vol. 22, No. 171, pp. 1258-1265 (September 1979).
25. Hutchinson, P. and Whalley, P.B., "A Possible Characterization of Entrainment in Annular Flow," Atomic Energy Research Establishment report AERE-R7126, Harwell, Berkshire, United Kingdom.
26. Collier, J. G. and Hewitt, G. F., "Data on the Vertical Flow of Air-Water Mixtures in the Annular and Dispersed Flow Regimes - Part II: Film Thickness and Entrainment Data and Analysis of Pressure Drop Measurements," Transactions of the Institute of Chemical Engineers, Vol. 39, 1961.
27. Gido, R. G., Grimes, C. I., Lawton, R. G., and Kudrick, J. A., "COMPARE: A Computer Program for the Transient Calculation of a System of Volumes Connected by Flowing Vents," Los Alamos Scientific Laboratory report LA-NUREG-6488-MS, September 1976.
28. Maerkl, H., "Study of the Process within a Multi-Partitioned Containment Model during Rupture of a Primary Cooling Circuit," U.S. Nuclear Regulatory Commission report NUREG/TR-0035, Vol. 2, September 1977.

29. "Subcompartment Pressure and Temperature Transient Analysis," Bechtel Power Corporation report BN-TOP-4, Rev. 1, October 1977.
30. Eckert, E. R. G. and Drake, Jr., R. M., Heat and Mass Transfer, 2nd Ed., (McGraw-Hill Book Co., 1959).

DISTRIBUTION

	Copies
Nuclear Regulatory Commission, R1, Bethesda, Maryland	298
Technical Information Center, Oak Ridge, Tennessee	2
Los Alamos Scientific Laboratory, Los Alamos, New Mexico	50
	350

NRC FORM 335 (7.77)

U.S. NUCLEAR REGULATORY COMMISSION

BIBLIOGRAPHIC DATA SHEET

1. REPORT NUMBER *(Assigned by DDC)*
NUREG/CR-1634
LA-8475-MS

TITLE AND SUBTITLE *(Add Volume No., if appropriate)*
Film Entrainment and Drop Deposition for Two-Phase Flow

2. *(Leave blank)*

3. RECIPIENT'S ACCESSION NO.

7. AUTHOR(S)
A. Koestel, R. G. Gido, J. S. Gilbert

5. DATE REPORT COMPLETED
MONTH July YEAR 1980

9. PERFORMING ORGANIZATION NAME AND MAILING ADDRESS *(Include Zip Code)*
Los Alamos Scientific Laboratory
P. O. Box 1663
Los Alamos, NM 87545

DATE REPORT ISSUED
MONTH August YEAR 1980

6. *(Leave blank)*

8. *(Leave blank)*

12. SPONSORING ORGANIZATION NAME AND MAILING ADDRESS *(Include Zip Code)*
Division of Systems Integration
Office of Nuclear Reactor Regulation
U. S. Nuclear Regulatory Commission
Washington, D. C. 20555

10. PROJECT/TASK/WORK UNIT NO.

11. CONTRACT NO.
FIN No. A7112

13. TYPE OF REPORT

PERIOD COVERED *(Inclusive dates)*

15. SUPPLEMENTARY NOTES

14. *(Leave blank)*

16. ABSTRACT *(200 words or less)*

A model for estimating the rate of film mass entrainment for drop-annular flow, based on film disturbance wave stability, was developed. The model was verified by application to tests involving deposition and entrainment. To account for the deposition, a recent particle mass diffusion correlation was used. Application of the entrainment and deposition models confirmed that a flow passage length (L/D) of about 100 or more is required to achieve near equilibrium, for a zero initial entrainment flow. The assumption of an initially fully entrained flow remaining approximately so, as used in nuclear power plant subcompartment analysis, is shown to be appropriate.

17. KEY WORDS AND DOCUMENT ANALYSIS

17a. DESCRIPTORS

17b. IDENTIFIERS/OPEN-ENDED TERMS

18. AVAILABILITY STATEMENT
Unlimited

19. SECURITY CLASS *(This report)*
Unclassified

21. NO. OF PAGES

20. SECURITY CLASS *(This page)*
Unclassified

22. PRICE
$